Process optimization and working fluid mixture design for organic Rankine cycles (ORCs) recovering compression heat in oxy-combustion power plants

Haoshui Yu[1], John Eason[2], Lorenz T. Biegler[2], Xiao Feng[3], Truls Gundersen[*1]

[1] Department of Energy and Process Engineering, Norwegian University of Science and Technology, Kolbjoern Hejes v. 1A, NO-7491 Trondheim, Norway

[2] Chemical Engineering Department, Carnegie Mellon University, Pittsburgh, PA 15213, United States

[3] School of Chemical Engineering & Technology, Xi'an Jiaotong University, Xi'an 710049, China

Abstract: In this study, an Organic Rankine Cycle (ORC) is proposed to be integrated with the flue gas pre-compression process to reduce the energy cost resulting from Carbon Capture and Storage (CCS). An equation-based flowsheet optimization model is developed considering the mixture working fluid design, ORC operating conditions and the compression process simultaneously. The optimal number of stages of CO_2 compression, the working fluid composition and the optimal operating conditions of ORCs and the compression train can be determined simultaneously using the proposed mathematical model. Proper heat integration can boost the power output of the ORC system significantly. The heat integration model considering variable process streams is extended to the integrated ORC and flue gas compression train process. The results show that the optimal number of stages is 4 and a pure working fluid could perform better than a mixture working fluid if operating conditions are chosen properly. The integration of ORCs can reduce the energy penalty by 7.9% compared with the original optimal design that did not include ORCs. In addition, one compressor stage is avoided.

Keywords: Carbon Capture and Storage (CCS), Compression Waste Heat, Organic Rankine Cycle, Process Integration, Mixture Working Fluid Design

1. Introduction

Due to climate change caused by human activity, the application of Carbon Capture and Storage (CCS) in the power industry has gained attention to reduce the greenhouse emissions. The penalties and costs are big challenges to apply CCS to the power industry [1]. There are three well-known configurations of power plants for carbon capture: post-combustion, pre-combustion and oxy-

* Corresponding author: truls.gundersen@ntnu.no

combustion. It is difficult to make a once-and-for-all decision on the best CO_2 capture option. Based on a techno-economic analysis and practical constraints, Kanniche et al. [2] suggested that Integrated Gasification Combined Cycle (IGCC) power plants should adopt pre-combustion capture by physical absorption, Natural Gas Combined Cycle (NGCC) plants should adopt post-combustion capture (amines), and Pulverized Coal power plants should adopt oxy-combustion. Oxy-combustion processes use high purity oxygen instead of air to combust the fuel, which facilitates the carbon capture process by removing most of the nitrogen before combustion. However, large energy penalties still exist in the carbon capture process for oxy-combustion coal-based power plants. The thermal efficiency penalty is about 9.4 %, which is mainly caused by the Air Separation Unit (ASU) and carbon dioxide compression and purification unit [3]. CO_2 needs to be compressed to a very high pressure (about 150 bar) for utilization and sequestration, which consumes a large amount of compression power. Compression heat is usually removed by cooling water due to its low temperature and thus results in significant energy losses. Measures to reduce this energy penalty should be taken. Fortunately, ORCs can convert low to medium temperature heat into power [4]. Solar energy [5], geothermal energy [6], biomass energy [7] and waste heat recovery in industry [8] are popular fields for ORC application.

Romeo et al. [9] proposed to use an ORC to recover the compression heat from the ASU and the CO_2 Compression and Purification Unit (CPU) in an oxy-combustion power plant. However, they just customized an ORC to recover waste heat in the system without optimization of the ORC and the compression process. Pei et al. [10] reviewed different CO_2 compression strategies and proposed to use an ORC to recover the compression heat. They compared 7-stage intercooling compression and 2-stage shockwave compression with and without waste heat recovery. The results indicate that without waste heat recovery, shockwave compression has a higher energy input requirement than the intercooling compression chain. However, with ORCs recovering waste heat, the shockwave compression case has a better performance. Optimization of the system is not performed in this study either. Esquivel-Patiño et al. [11] integrated an ORC with the NGCC power plant and carbon capture system. Only one working fluid R245fa was used in this study. The operating conditions of the NGCC power plant are fixed, which may lead to non-optimal design. Aneke and Wang [12] investigated the potential of improving the energy efficiency in a cryogenic ASU through recovering the waste heat by an ORC. They performed the modeling using process simulators. They compared 3-stage and 1-stage air compression waste heat recovery using an ORC. Lee and Han [13] proposed to use an ORC to utilize the waste heat from a post-combustion carbon capture process. However, they mainly focused on Liquefied Natural Gas (LNG) cold energy utilization. The process optimization is performed through exergy analysis and use of the Grand Composite Curve (GCC) in an iterative way. Kurtulus et al. [14] performed thermoeconomic analysis of a CO_2 compression system using waste heat into the regenerative organic Rankine cycle. However, the number of compression stages is fixed at 7 stages and process optimization is not taken into consideration in this study.

In an ORC, the working fluid exerts great influence on the system performance. One of the disadvantages of an ORC with a pure working fluid for sensible waste heat recovery is the isothermal phase change, which results in a severe pinch limitation [15]. Mixture working fluids with non-isothermal phase change are an option to alleviate the pinch limitation. Zeotropic mixture working fluids could significantly improve the overall efficiency of the system. As the non-isothermal phase change results in temperature glide, the mixture working fluid can match better with the heat source/sink temperature profile. Therefore, zeotropic mixtures as working fluids for ORCs have received increasing attention. Anglino and Colonna di Paliano [16] analyzed a mixture of n-butane and n-hexane as a working fluid for a geothermal ORC. The results showed that 6.8% more power is produced compared to pure n-pentane. Liu et al. [6] investigated the performance of a geothermal ORC using R600a/R601a mixtures as working fluid, and the results show that 4-11% more power can be generated compared with an ORC using pure R600a. More waste heat can be recovered by the organic working fluid. In the studies authored by Wang et al. [17] and Wang and Zhao [18], the mixture of R245fa/R152a is investigated. Heberle et al. [19] investigated the mixture of iso-butane/iso-pentane and R227ea/R245fa. Other combinations of working fluids are investigated in the open literature as well, but it should be noted that the boiling point difference cannot be too large or too small. Too large boiling point difference may lead to the fractionation phenomenon in the evaporator of an ORC [20], while a small boiling point difference may cause a very small temperature glide, which cannot considerably improve the thermal match between waste heat and the working fluid. Zhou et al. [21] discussed the composition shift of zeotropic mixture working fluids in ORCs. The reasons for composition shift are well explained in their study. The relationship between temperature glide and composition shift is revealed as well. Yu et al. [22] investigated the integration of heat pump and ORC to increase the net power generation. If the working fluid in the ORC is chosen appropriately, the integration of a heat pump can boost the power output significantly. It can be seen that the candidate composition of mixture working fluids should be chosen carefully. Even though several studies focus on ORCs recovering waste heat from flue gas compression processes, the simultaneous optimization of a carbon capture process and an ORC has not been reported, not to mention the mixture working fluid design in this process.

To address the above issues and reduce the energy penalty from the carbon capture process, simultaneous optimization of an ORC and the carbon capture process should be performed. In this study, we address two gaps in literature. First, few studies have considered the simultaneous optimization of the carbon capture process and an ORC. Second, the mixture working fluid design along with process optimization has not been reported in the open literature. In this study, an equation-oriented mathematical model for simultaneous optimization of carbon capture process, mixture working fluid design, and operating conditions of an ORC recovering waste heat from the compression process in an oxy-combustion power plant is presented.

2. Problem statement

In an oxy-combustion coal-based power plant, the CO_2 rich flue gas must be conditioned and compressed to high pressure (around 150 bar) for utilization or sequestration. Fu and Gundersen [23] optimized and compared the sub-ambient CO_2 conditioning process for one-stage, two-stage and three-stage flash units. Based on the two-stage flash unit system, Dowling et al. [24] reoptimized the flowsheet as shown in Figure 1. This flowsheet can be classified into three zones, a pre-compression zone with intercooling, a flash and purification zone with two flash vessels, and the remaining section for carbon dioxide compression/pumping. Among these three sections, the pre-compression zone consumes large amount of electricity and generates relatively high temperature waste heat. The compression power consumption of the whole flowsheet is minimized subject to purity and recovery requirements. The heat exchange units in the flash and purification Zone (Heat Exchanger Zone 2 in reference [24]) are assigned to a multistream heat exchanger and integrated with other process units. The heat exchange units in the third zone are assigned to the chilled water zone, where the streams can be cooled by chilled water. These streams are the waste heat sources that can be recovered by an ORC to improve the energy efficiency of the system. However, due to the very high pressure after FT3, CO_2 is in dense phase and the compression heat has a very low temperature (around 310 K). Such waste heat is not worth recovering with an ORC.

The compression waste heat from the initial state to purification and flash zone (yellow shaded area indicated in Figure 1) is at high enough temperature. This region represents a 5-stage pre-compression of flue gas. In the final optimal design, there are five stages to compress flue gas from 1.03 bar to 28.33 bar.

In this study, we intend to customize an ORC to recover the compression heat from the pre-compression zone as shown in Figure 1. The optimal number of compression stages can alter if an ORC is customized to this system. Fewer stages of compression can elevate the temperature of compression heat, and thus may result in higher power output of the ORC. Therefore, the trade-off between carbon capture power consumption and the ORC power output should be considered. To improve the thermal efficiency of an ORC, mixture working fluids will be considered, and the composition of the organic working fluid and ORC operating conditions should be optimized simultaneously with the flue gas compression process. For detailed results of the process, please refer to [24].

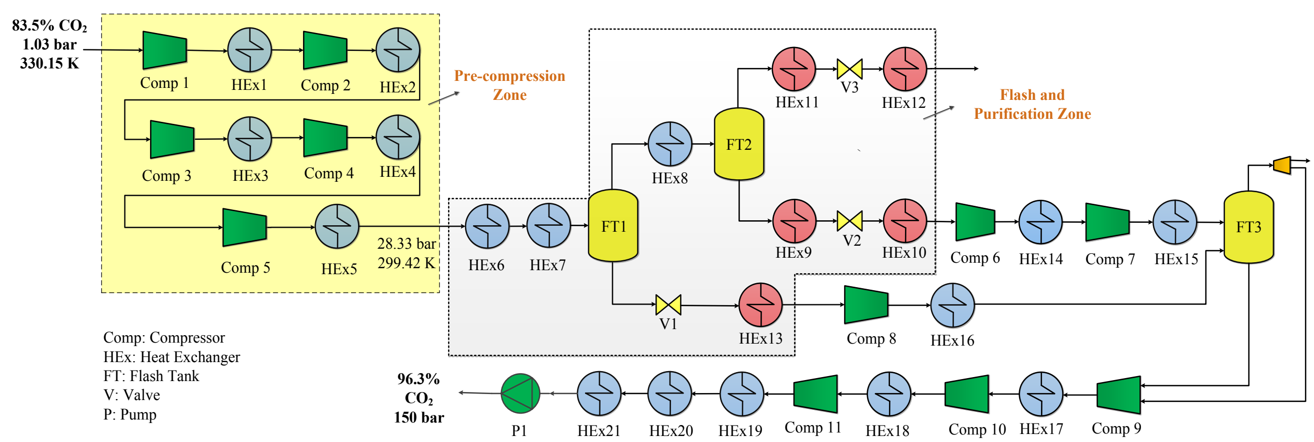

Fig. 1 The flowsheet of carbon dioxide conditioning and compression in an oxy-combustion power plant (modified from [24])

3. Process modelling and optimization

To optimize the integrated system, an equation oriented mathematical model is constructed in the General Algebraic Modeling System (GAMS) [25] environment. The nonlinear optimization solver CONOPT [26] is selected as the solver for the proposed model. The mathematical model incorporates the following sub-models: (1) a rigorous thermodynamic model to calculate the properties of the working fluid and flue gas; (2) an ORC model to determine the optimal working fluid composition and operating conditions; (3) a flue gas compression model to determine the optimal number of stages and compression ratios; (4) the Duran-Grossmann model [27] to determine the heat integration between the ORC and the waste heat from the flue gas compression. These sub-models jointly determine the final optimal design of the integrated system.

3.1 Thermodynamic property model

Thermodynamic property calculations are the most computationally challenging in both process simulation and optimization. To get a reliable optimal design of the integrated system, rigorous thermodynamic models must be built to calculate the properties of the flue gas and the organic working fluid in the ORC. In this study, an equation-oriented approach is adopted to model the whole system, which has some advantages over commercial sequential modular methods [28]. Compared with sequential modular methods, the equation-oriented approach enables simultaneous optimization and convergence of the flowsheet and exploits advances in mathematical programming, such as efficient large-scale solvers, modeling discrete events and decisions, optimization decomposition algorithms and low cost sensitivity analysis [28]. For the thermodynamic properties of the flue gas and working fluids in the ORC, a Cubic Equations of State (CEOS) is adopted. The general form of a CEOS is shown in Eq. (1).

$$Z^3-(1+B-uB)Z^2+(A+wB^2-uB-uB^2)Z-AB-wB^2-wB^3=0 \quad (1)$$

Where Z is the compressibility factor, A and B are dimensionless coefficients related to temperature, pressure and composition. u and w are constants depending on the actual CEOS. In this study, the Peng-Robinson equation is chosen to calculate the thermodynamic properties, since the Peng-Robinson equation has large applicability ranges in terms of temperature and pressure and balances computational expense and accuracy. For the Peng-Robinson equation, $u=2$ and $w=-1$. The detailed information for the Peng-Robinson equation is provided in Appendix.

Since the CEOS can have up to 3 real roots, the correct root selection is important for the thermodynamic property calculation. Kamath et al. [29] proposed a strategy to map the roots of CEOS to the correct state. The vapor phase corresponds to the largest real root while the liquid phase corresponds to the smallest real root. Based on this observation, the first and second derivatives of the cubic equation in Eq. (1) can be used to determine the correct root [30]. Therefore, the sets of state points SP, liquid state points LSP and gas state points GSP are defined to facilitate the root mapping. Eq. (2) is used to exclude the spurious middle root of the CEOS. A nonnegative second derivative denotes the vapor phase, and a non-positive second derivative denotes the liquid phase. Eq. (3) and (4) assign the correct root to the gas phase and liquid phase respectively.

$$f'(Z_{sp})=3Z_{sp}{}^2+2(B-1)Z_{sp}+(A-2B-3B^2)\geq 0 \quad \forall sp\in SP \quad (2)$$

$$f''(Z_{sp})=6Z_{sp}+2(B-1)\geq 0 \quad \forall sp\in GSP \quad (3)$$

$$f''(Z_{sp})=6Z_{sp}+2(B-1)\leq 0 \quad \forall sp\in LSP \quad (4)$$

Then the thermodynamic properties enthalpy (h_s) and entropy (S_s) are calculated using departure functions as follows,

$$h_s - h_s^0 = (a_s^m - T_s \frac{\partial a_s^m}{\partial T_s}) \frac{1}{b_s^m \sqrt{u^2 - 4\omega}} \ln \left[\frac{2Z_s + B_s(u - \sqrt{u^2 - 4\omega})}{2Z_s + B_s(u + \sqrt{u^2 - 4\omega})} \right] + RT_s(Z_s - 1) \quad (5)$$

$$S_s - S_s^0 = R \ln(\frac{Z_s + B_s}{Z_s}) + R \ln(\frac{Z_s P^0}{P_s}) - \frac{\partial a_s^m}{\partial T_s} \frac{1}{b_s^m \sqrt{u^2 - 4\omega}} \ln \left[\frac{2Z_s + B_s(u - \sqrt{u^2 - 4\omega})}{2Z_s + B_s(u + \sqrt{u^2 - 4\omega})} \right] \quad (6)$$

$$\frac{\partial a_s^m}{\partial T_s} = -\frac{R}{2} \sqrt{\frac{\Omega_a}{T_s}} \sum_{i \in C} \sum_{j \in C} x_i x_j (1 - k_{i,j}) \left[f_{\omega,j} \sqrt{\frac{a_i T_{j,c}}{P_{j,c}}} + f_{\omega,i} \sqrt{\frac{a_j T_{i,c}}{P_{i,c}}} \right] \quad (7)$$

$$h_s^0 = \sum_{c \in C} x_c \left[\frac{C_c^V}{5}(T^5 - T_0^5) + \frac{C_c^{IV}}{4}(T^4 - T_0^4) + ... + C_c^I (T - T_0) \right] \quad (8)$$

$$S_s^0 = \sum_{c \in C} x_c \left[\frac{C_c^V}{4}(T^4 - T_0^4) + ... + C_c^I \ln(\frac{T}{T_0}) \right] \quad (9)$$

Where a^m and b^m are mixture properties. Mixing rules with binary interaction parameters are adopted, which can be found in Appendix. Finally the fugacity coefficient is defined as follows.

$$\ln(\phi_i) = \frac{b_i}{b_s^m}(Z - 1) - \ln(Z - B) + \frac{A}{B\sqrt{u^2 - 4\omega}} (\frac{b_i}{b_s^m} - \delta_i) \ln \left[\frac{2Z_s + B_s(u - \sqrt{u^2 - 4\omega})}{2Z_s + B_s(u + \sqrt{u^2 - 4\omega})} \right] \quad (10)$$

$$\delta_i = \frac{2\sqrt{a_i}}{a_s^m} \sum_{j \in C} x_j \sqrt{a_j} (1 - k_{i,j}) \quad (11)$$

The detailed parameters used for thermodynamic property calculation are provided in Appendix.

3.2 ORC model with mixture working fluid

Figure 2 illustrates the layout of an ORC and the corresponding T-S diagram. There are four processes in an ORC: (I) pumping the working fluid to the evaporation pressure; (II) isobaric heat addition in the evaporator; (III) expansion and power generation from the turbine; (IV) isobaric heat rejection in the condenser. To model the heat transfer behavior between the flue gas and the organic working fluid, the evaporation process can be divided into three sections, namely preheating section (2 to 3), evaporating section (3 to 4) and superheating section (4 to 5). If a mixture working fluid is used, the bubble point (state point 1and 3) and dew point (state point 4 and 7) offer a temperature glide to match better with the waste heat source and chilled water. Based on previous studies [31, 32], three working fluids as listed in Table 1 are considered as components for the mixture working fluid. The corresponding critical properties and environmental parameters are also given in Table 1.

Table 1 Working fluids used in this study

Working fluid	Chemical formula	Tc (K)	Pc (bar)	ODP[a]	Type
R227ea	C_3HF_7	374.83	29.12	0.0	Dry
R152a	$C_2H_4F_2$	386.44	45.20	0.0	Wet
R245fa	$C_3H_3F_5$-D1	427.20	36.40	0.0	Isentropic

[a] Ozone Depletion Potential

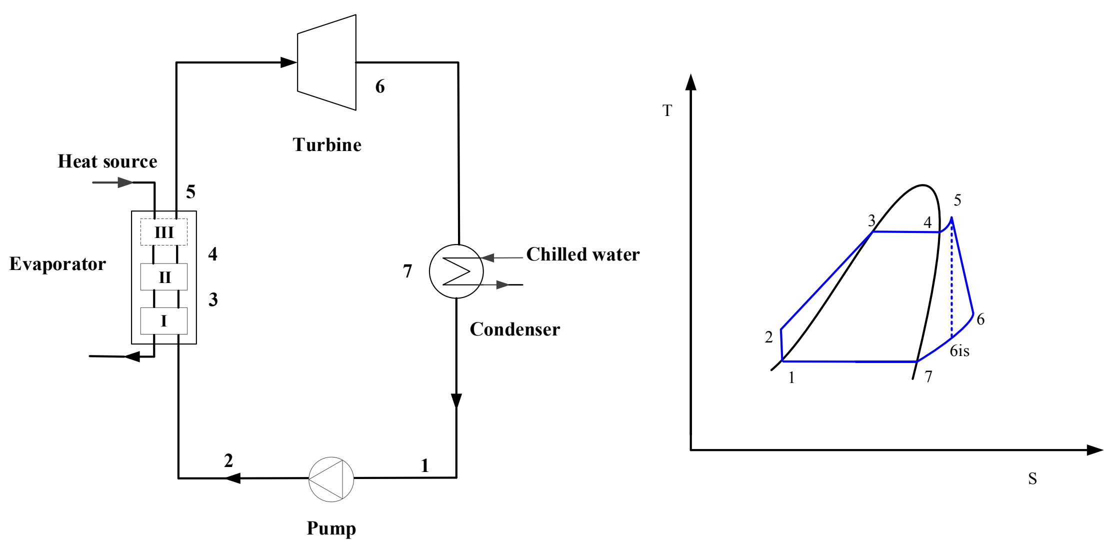

Fig. 2 Flowsheet and T-S diagram of an ORC

To facilitate formulation of the ORC model, the state point set $SP = \{1, 2, 3, \ldots 7\}$ is defined referring to the different ORC state points as shown in Figure 2. However, state points 4 and 5 may coincide if non-superheating is preferable. The state point set $SP = \{1, 2, 3, \ldots 7\}$ can be classified into two subsets, namely liquid state points $LSP=\{1,2,3\}$ and gas state points $GSP=\{4,5,6,6is,7\}$. In addition, state points 1, 3, 4, and 7 are at a saturated state, and a corresponding set may be defined as $SSP=\{1,3,4,7\}$. Even though the composition of all the state points in the ORC are the same, phase equilibrium calculations are required because the bubble and dew point temperatures are significant for the system. The bubble and dew points reflect the temperature glide of the mixture working fluids. Phase equilibrium can be calculated using a shadow (i.e., hypothetical) point. Each of the saturated state points is assigned to a shadow point denoted *shdw* following the state point. Shadow points are used to calculate the bubble point and dew point properties, even though these shadow points do not exist in reality.

For the ORC system, each state point has the same composition and the summation of molar fractions should satisfy Eq. (12).

$$\sum_{c\in C} x_{c,p} = 1 \quad \forall p \in SP \tag{12}$$

where c represents the components in the mixture working fluid, and x is the molar fraction of component c at state point p.

For the dew and bubble points, the phase equilibrium should be calculated. Eq. (13) is the equilibrium expression for saturated liquid state points 1 and 3. Similarly, Eq. (14) is the equilibrium expression for saturated gas state points 4 and 7. The corresponding fugacity coefficients in Eqs. (13) and (14) are calculated through the thermodynamic model.

$$\left.\begin{aligned} x_{c,i}\phi^{L}_{c,i} &= x_{c,i,shdw}\phi^{V}_{c,i,shdw} \\ T^{L}_{i} &= T^{V}_{i,shdw} \\ P^{L}_{i} &= P^{V}_{i,shdw} \end{aligned}\right\} \quad if\ i=1,3 \tag{13}$$

$$\left.\begin{array}{l} x_{c,i,shdw}\phi^{L}_{c,i,shdw} = x_{c,i}\phi^{V}_{c,i} \\ T^{L}_{i,shdw} = T^{V}_{i} \\ P^{L}_{i,shdw} = P^{V}_{i} \end{array}\right\} \quad if\ i = 4,7 \tag{14}$$

Where ϕ denotes the fugacity.

Then the turbine performance is modeled based on an isentropic efficiency by using a hypothetical isentropic point. The isentropic state point 6is has the same pressure as state point 6, yet the same entropy as the turbine inlet state point 5 as shown in Eqs. (15)-(16). Then isentropic efficiency is calculated through Eq. (17) and the power output can be obtained through Eq. (18), where f_{wf} is the molar flowrate of working fluid.

$$S_5 = S_{6is} \tag{15}$$

$$P_6 = P_{6is} \tag{16}$$

$$\eta_{is} = (h_5 - h_6)/(h_5 - h_{6is}) \tag{17}$$

$$W_{tur} = f_{wf}(h_5 - h_6) \tag{18}$$

The power consumed by the pump is calculated by Eq. (19):

$$W_{pump} = \frac{f_{wf}(h_2 - h_1)}{\eta_{pump}} \tag{19}$$

where η_{pump} is assumed to be 100% based on the assumption of isentropic pumping process.

The net power output of the ORC is calculated by Eq. (20).

$$W_{ORC} = W_{tur} - W_{pump} \tag{20}$$

The evaporation process of the organic working fluid will be integrated with the compression heat from the flue gas compression process. Then the evaporation process is considered in the heat integration model.

3.3 Flue gas compression model

In the original work, the treated and dried flue gas (83.5 mol% CO_2) is fed to the carbon capture and compression unit using five stage compressors with intermediate cooling [24]. The waste heat is cooled to 288.15 K by chilled water. The flue gas is composed of 83.5 mol% CO_2, 3.5 mol% Ar, 10 mol% N_2 and 3 mol% O_2. The flue gas is compressed from 1.03 bar to 28.33 bar as shown in Figure 1. In this study, these assumptions are maintained, but the number of stages is allowed to vary. The fewer stages, the higher quality of waste heat when customizing an ORC. In this study, 3, 4 and 5 compression stages will be investigated when integrated with an ORC. Figure 3 illustrates 4 stages of flue gas compression.

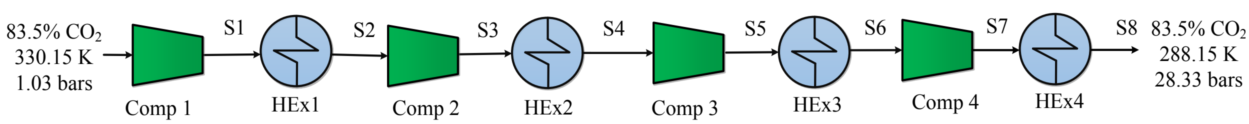

Fig. 3 Four stages compression of flue gas in an oxy combustion power plant

The flue gas compression process is modelled by Eqs (21)-(30). For any compressors the following isentropic calculation is performed. The isentropic efficiency of the compressors is assumed to be 82%. There is a shadow stream with the isentropic compression. In the flue gas compression sub-model, *comp* denotes the compressors in the compression train. Then the pressure ratio is also a variable in this process. The corresponding power consumption is calculated by Eq. (29) and (30), where f_{fg} is the molar flowrate of flue gas.

$$T_{in,comp} \leq T_{out,comp} \tag{21}$$

$$P_{in,comp} \leq P_{out,comp} \tag{22}$$

$$P_{out,comp} \leq P_{out,comp+1} \tag{24}$$

$$P_{out,comp} = P_{in,comp+1} \tag{25}$$

$$h_{out,comp} - h_{in,comp} = \frac{1}{\eta_{is}}(h_{out,comp,is} - h_{in,comp}) \tag{26}$$

$$S_{out,comp,is} = S_{in,comp} \tag{27}$$

$$P_{out,comp,is} = P_{out,comp} \tag{28}$$

$$W_{comp} = \frac{f_{fg}}{\eta_{mech}}\left(h_{out,comp} - h_{in,comp}\right) \tag{29}$$

$$W_{CPU} = \sum_{comp \in COMP} W_{comp} \tag{30}$$

3.4 Heat integration model

Good heat integration between compression waste heat and the ORC will boost the power output of the system. The mixture working fluid acts as a cold stream, and the compression waste heat sources act as hot streams. However, both the waste heat and the ORC have variable flowrates and temperatures. Due to phase change of the working fluid, the pinch points between waste heat and the organic working fluid can occur at the bubble point of the working fluid (state point 3). Hence, the working fluid should be decomposed into sub streams to perform correct heat integration. The working fluid is decomposed into 3 substreams, namely a subcooled stream, a two-phase stream and a superheated stream. However, the superheated stream may disappear if superheating is not favored. The number of compression stages determines how many hot streams there are in the system. If 5-stage compression is considered, then there are 5 hot streams, etc. Since both the hot and cold stream properties are variables, classical heat integration technology cannot handle this problem, instead the Duran-Grossmann model [27] is adopted. This model has been successfully applied to an ORC recovering waste heat in refineries [33]. To introduce this model, the 4-stage compression in Figure 3 is used as an example. There are 4 hot streams from compression and 3 cold streams from the ORC working fluid. The hot stream set is defined as $I = \{H1, H2, H3, H4\}$

and the cold stream set is defined as $J=\{C1,C2,C3\}$. The union of set I and J is defined as $S=I\cup J$. The streams in Table 2 are defined as the streams involving in heat integration.

Table 2. Streams involved in the heat integration with 4-stage compression

Stream	State points	Inlet temperature	Outlet temperature	Heat load
C1	2→3	T_2	T_3	$f_{wf}(h_3-h_2)$
C2	3→4	T_3	T_4	$f_{wf}(h_4-h_3)$
C3	4→5	T_4	T_5	$f_{wf}(h_5-h_4)$
H1	S1→S2	T_{S1}	T_{S2}	$f_{fg}(h_{S1}-h_{S2})$
H2	S3→S4	T_{S3}	T_{S4}	$f_{fg}(h_{S3}-h_{S4})$
H3	S5→S6	T_{S5}	T_{S6}	$f_{fg}(h_{S5}-h_{S6})$
H4	S7→S8	T_{S7}	T_{S8}	$f_{fg}(h_{S7}-h_{S8})$

In the Duran-Grossmann model, the inlet temperatures of hot streams are considered as pinch candidates. For cold streams, the pinch candidate temperatures are the inlet temperatures plus a minimum approach temperature $\Delta T_{\min}$.

$$T_i^p=T_i^{in} \quad \forall i\in I \tag{31}$$

$$T_j^p=T_j^{in}+\Delta T_{\min} \quad \forall j\in J \tag{32}$$

The set of pinch candidates is defined as $PC=\{T_s^p\,|\forall s\in S\}$, thus the heat load of all the hot and cold streams above each pinch candidate can be calculated by Eqs. (33) and (34) respectively.

$$QSOA(x)^p=\sum_{i\in I}FCP_i\left[\max\left\{0,T_i^{in}-T^p\right\}-\max\left\{0,T_i^{out}-T^p\right\}\right] \quad \forall i\in I \tag{33}$$

$$QSIA(x)^p=\sum_{j\in J}FCP_j\left[\max\left\{0,T_j^{out}-(T^p-\Delta T)\right\}-\max\left\{0,T_j^{in}-(T^p-\Delta T)\right\}\right] \quad \forall j\in J \tag{34}$$

The heat deficit above each pinch candidate can be calculated by Eq. (35).

$$Z_H^p(x)=QSIA(x)^p-QSOA(x)^p \quad \forall p\in PC \tag{35}$$

Then the pinch point is identified as the pinch candidate with maximum heat deficit. The corresponding hot utility requirement can be calculated by Eq. (36).

$$Z_H^p(x) \le Q_{HU} \quad \forall p \in PC \tag{36}$$

Then the cold utility requirement can be determined by an overall heat balance as shown in Eq. (38).

$$Q_{CU} = Q_{HU} + \sum_{i \in I} FCp_i (T_i^{in} - T_i^{out}) - \sum_{j \in J} FCp_j (T_j^{out} - T_j^{in}) \tag{38}$$

In Eqs. (33) and (34) there are max operators that cannot be handled by most continuous optimization algorithms. Thus, the max operators are reformulated by smooth functions [34], as shown in Eq. (39).

$$\max\{0, x\} \approx \frac{1}{2}(x + \sqrt{x^2 + \varepsilon}) \tag{39}$$

where ε is a small constant, typically between 10^{-3} and 10^{-6}.

3.5 Objective function and the overall model

The objective is to minimize net power consumption of the system. However, in this application the hot utility should be zero since an ORC aims at recovering waste heat instead of consuming hot utility to generate power. To drive hot utility to 0 and prevent the ORC consuming hot utility to generate power, a penalty term related to hot utility is incorporated in the objective function, which is defined as follows (where M is a sufficiently large number):

281 $$obj = W_{CPU} - W_{ORC} + M \bullet Q_{HU}$$

Based on the above sub-models, the integrated ORC and flue gas compression train can be formulated as the following nonlinear program:

$$
\begin{aligned}
&\min_{x\in\Omega} \quad obj \\
&\text{s.t.} \\
&\Omega = \left\{ x \,\middle|\, \begin{array}{l} \text{thermodynamic model Eqs.(1)-(11)} \\ \text{ORC model Eqs.(12)-(20)} \\ \text{flue gas compression model Eqs.(21)-(30)} \\ \text{heat integration model Eqs.(31)-(39)} \end{array} \right\}
\end{aligned}
$$

4. Results and discussion

To avoid numerical problems from the large magnitude of flue gas flowrate, the flowrate is assumed to be 100 mol/s in the model. The corresponding industrial data can be rescaled based on the results from this model. The mathematical model was solved using GAMS-CONOPT. The optimal results with different number of compression stages are listed in Table 3. The first row of Table 3 indicates the minimum compression work without considering an ORC. It is clear and straightforward that when reducing the number of compression stages, the compression work increases. The second row of Table 3 illustrates the compression work considering an ORC at the optimal solution. It can be seen that for 5-stage compression, the compression work is almost the same with/without customizing an ORC (107.31kW vs.107.32 kW), which means the introduction of the ORC exerts little influence on the compression train. For 4-stage and 3-stage compression, the compression work considering an ORC is greater than the compression work without considering an ORC. The reason is as follows: since the ORC favors higher temperature heat source, the compression process tends to consume more power to obtain higher temperature compression heat. This indicates that the increase of an ORC power generation overweighs the compression work increase in this system. It is clear that 4-stage compression is the optimal strategy with minimum power consumption.

Table. 3 Optimization results for varying number of compression stages

Variable	5-stage	4-stage	3-stage	4-stage with evaporation pressure limitation
Minimum compression work without ORC (kW)	107.31	110.57	116.13	110.57
Optimal compression work with ORC (kW)	107.32	112.71	123.97	114.94
Optimal power output of ORC (kW)	5.81	16.05	25.20	16.10
Optimal net power consumption with ORC (kW)	**101.51**	**96.66**	**98.77**	**98.84**
Hot utility (kW)	0	0	0	0
Cold utility (kW)	50.2	2.99	2.56	7.47
Working fluid composition (R227ea/R152a/R245fa)	1/0/0	1/0/0	0/0/1	1/0/0
Working fluid molar flowrate (mol/s)	3.42	5.60	4.30	5.19
ORC evaporation pressure (bar)	8.79	29.11	36.4	28
ORC evaporation temperature (K)	321.63	374.82	427.19	372.84
Degree of superheating (K)	-	-	-	-
Waste heat recovered (kW)	80.12	132.72	144.06	130.40

The corresponding stream data for heat integration are listed in Table 4. Surprisingly, the optimal working fluid is pure R227ea instead of a mixture working fluid. This deserves further investigation of the system. The operating condition is at the critical point of R227ea. This means that the working fluid has no-latent heat evaporating process, which explains why the pure working fluid R227ea outperforms the mixture working fluids because no phase change taking place under these conditions. Therefore, only one cold stream C1 occurs in heat integration, as shown in Table 4. The corresponding Composite Curves are shown in Figure 4.

Table 4. Optimal stream data of the integrated system with 4-stage compression

Stream	State points	Pressure (bar)	Inlet temperature (K)	Outlet temperature (K)	Heat load (kW)
C1	2→3	29.12	289.56	374.82	132.72
H1	S1→S2	1.73	379.33	294.56	-31.51
H2	S3→S4	4.50	381.37	294.56	-32.65
H3	S5→S6	11.40	379.33	293.82	-33.07
H4	S7→S8	28.33	379.33	288.15	-38.46

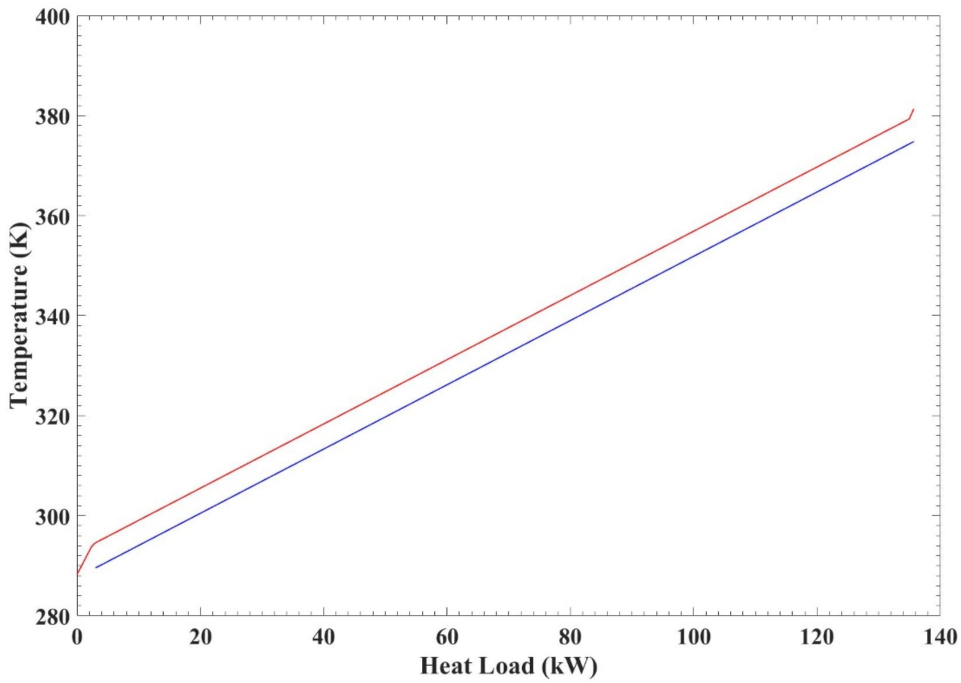

Fig. 4 Composite Curves of the system with 4-stage compression

It can be seen that the ORC optimization converges to the critical point of R227ea, but this may cause operation problems. In addition, the heat transfer behavior is unknown in the critical region for the organic working fluids. The temperature is very sensitive to pressure near the critical point. Even though an ORC with pure working fluid R227ea operating near the critical point performs best, the actual implementation is quite difficult in practice.

To guarantee a practical solution of the model, a constraint on the evaporating pressure is added to confine the operating conditions to a rational and controllable region. We set the upper bound of the evaporation pressure to 28 bar, which is less than the critical pressure of R227ea (29.12 bar). The solution of the model with a constraint on the evaporation pressure is listed in the last column of Table 3. It is obvious that the net power consumption of 4-stage compression with an evaporation pressure constraint increases compared with the scheme without the pressure constraint. The net power consumption is slightly higher than that of 3-stage compression. It should be noted that 3-stage compression favors pure working fluid R245fa. The evaporation pressure is 36.4 bar, which is the critical pressure of R245fa. This indicates that the operating conditions converge to the critical point of R245fa with 3-stage compression. The same operational and practical problems apply to the 3-stage compression as well. If another evaporation pressure constraint is added to the model with 3-stage compression, the net power consumption will increase. Therefore, the 4-stage compression with evaporation pressure constraint is a practical solution since the evaporation pressure is slightly less than the critical pressure and the net power consumption is low. The corresponding process streams are listed in Table 5. It can be seen that there is phase change under this circumstance. The corresponding Composite Curves (CCs) and Grand Composite Curve (GCC) are shown in Figures 5 and 6. The cold utility is 7.47 kW. Based on the operating conditions and the GCC, the compression waste heat should be cooled from 294.5 K to their target temperatures. There are two pinch points in this system, which indicates an energy intensive process. The final design is illustrated in Figure 7. It can be seen that the composition of working fluid is still pure working fluid R227ea because R227ea evaporating at 28 bar has a small ratio of latent to sensible heat. The ratio is 0.16=18.19/112.19. This parameter is very important for ORC systems recovering waste heat without target temperature constraints. Compared with the original 5-stage compression (107.31 kW), the net power consumption is 98.83 kW with the pressure constraint. Therefore, the net power consumption is decreased by 7.9%.

Table 5. Stream data with optimal operating conditions for 4-stages with evaporation pressure constraint.

Stream	State points	Pressure (bar)	Inlet temperature (K)	Outlet temperature (K)	Heat load(kW)
C1	2→3	28	289.50	372.84	112.2
C2	3→4	28	372.84	372.84	18.2
H1	S1→S2	1.73	385.64	288.15	-36.2
H2	S3→S4	4.50	395.05	341.03	-20.9
H3	S5→S6	11.40	383.60	288.15	-36.5
H4	S7→S8	28.73	392.87	288.15	-44.1

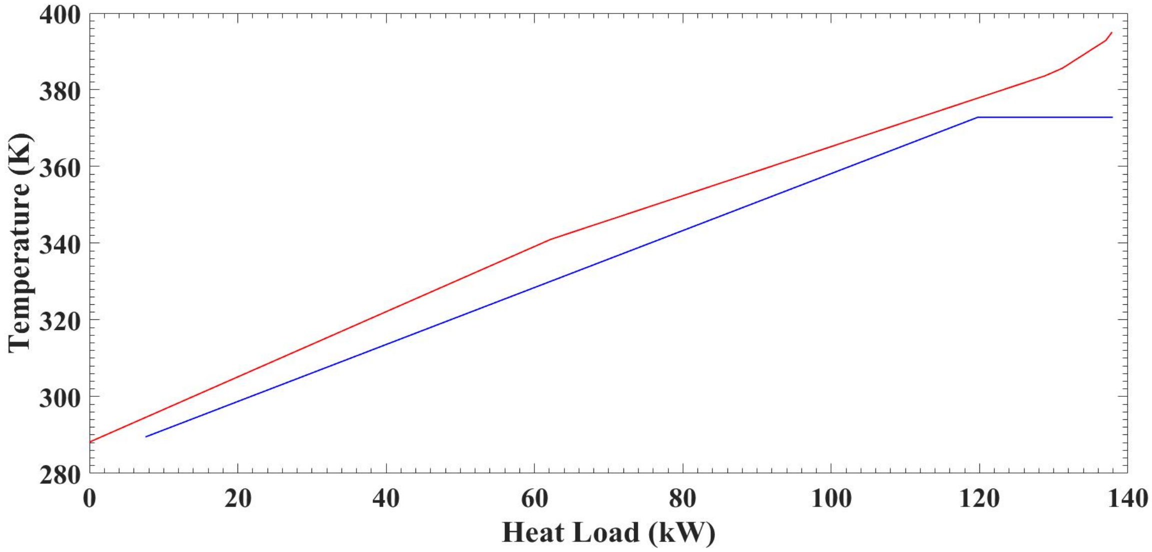

Fig. 5 Composite Curves of 4-stage compression with evaporation pressure constraint

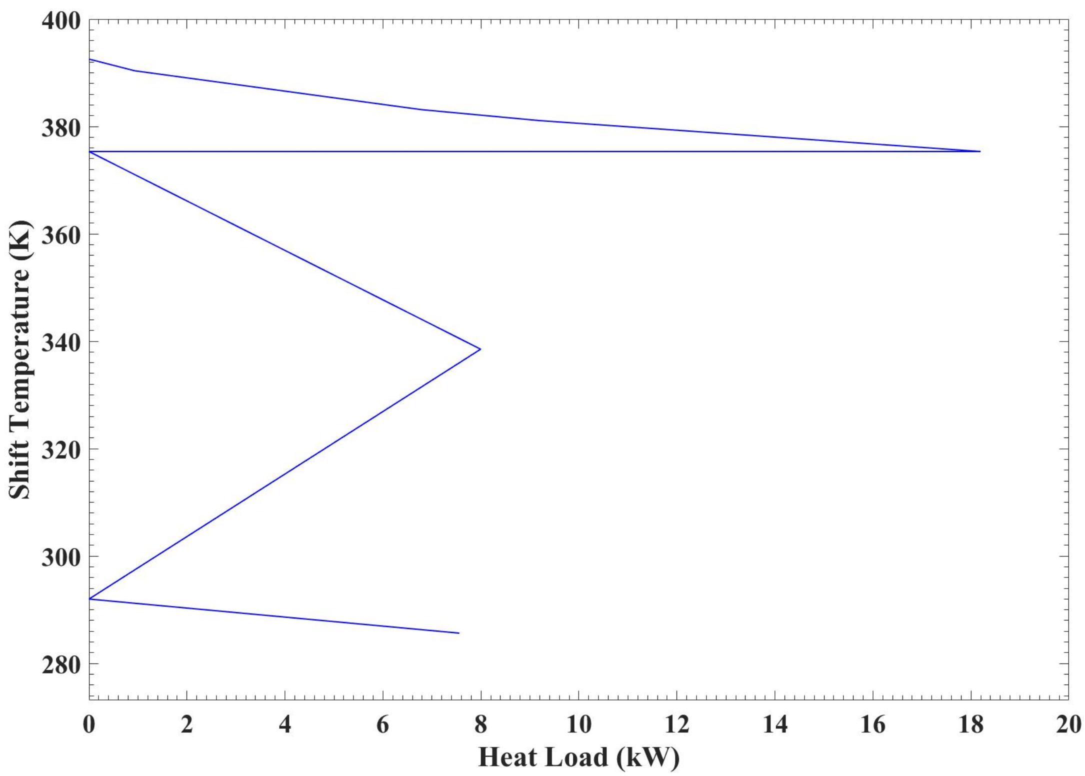

Fig. 6 Grand Composite Curve of 4-stage compression with evaporation pressure constraint

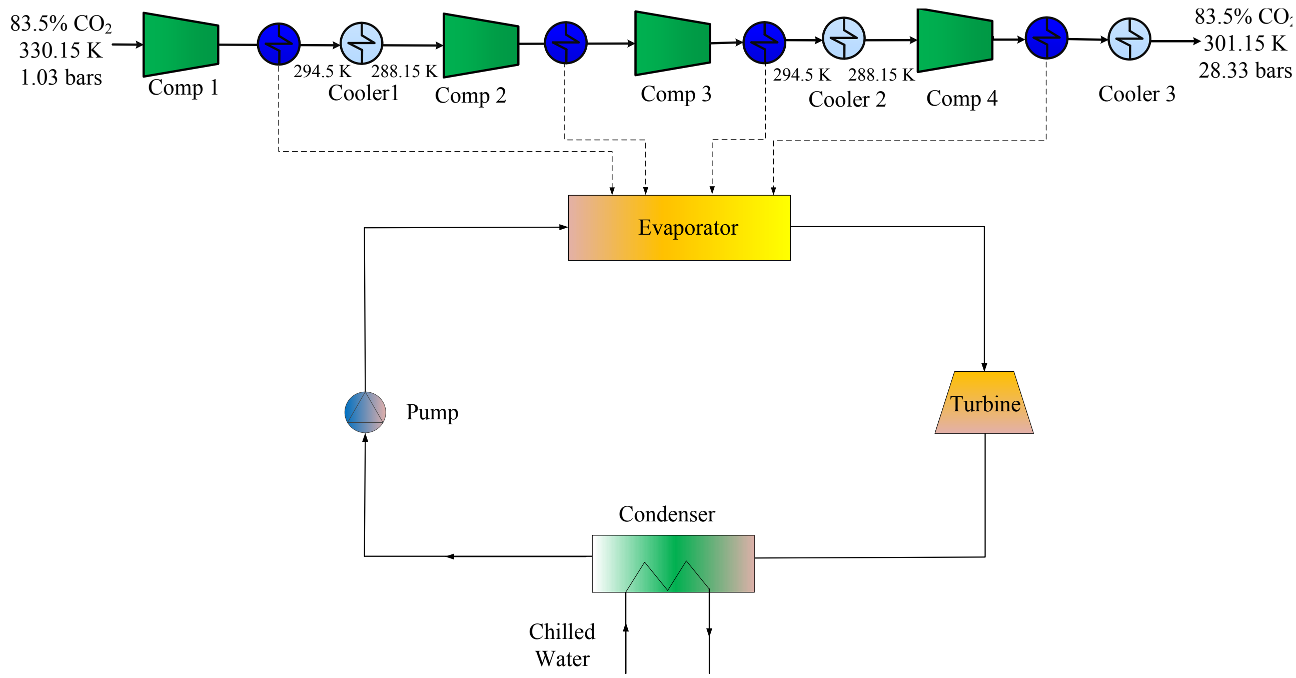

Fig. 7 The design of 4-stage compression waste heat recovery

The results show that pure working fluids evaporating near critical region perform better than mixed working fluids due to the small latent heat. This indicates that increasing the evaporation pressure to the critical pressure can decrease or eliminate the latent heat of phase change, which further implies that a transcritical ORC may perform better than a subcritical ORC. Transcritical ORCs have higher thermal efficiency and better thermal match between the heat source and the working fluid. However, the heat transfer characteristics of working fluids in the pseudocritical region are quite different from subcritical ORCs. Thermophysical properties are very sensitive to the operating conditions in the pseudocritical region, so heat exchanger design is a challenging task for transcritical ORCs [35]. Few studies are available on the reliable thermophysical properties of working fluids in the pseudocritical region. Another option is to configure the ORC to a pressure close to but below critical pressure as adopted in the 4-stage compression with pressure constraint design. An ORC with pure working operating in this operating region performs better than an ORC with a mixture working fluid. The mixture working fluid may perform better if there is no working fluid like R227ea whose critical temperature is lower than the waste heat inlet temperature. If all the working fluid candidates have higher critical temperature, a mixture working fluid would perform better. This finding also provides guidance in working fluid selection. The working fluid of an ORC for sensible waste heat recovery should be the one whose critical temperature is lower than the waste heat inlet temperature. These pure component working fluids evaporate at pressures close to their critical pressure perform better than mixture working fluids.

5. Conclusions

An ORC system is proposed to recover the waste heat generated from flue gas compression in an oxy-combustion coal-based power plant. An equation-oriented mathematical model is established to optimally integrate an ORC with the carbon capture process. The mathematical model consists of 4 sub-models: a thermodynamic property model, an ORC model, a flue gas compression model and a heat integration model. This model optimizes the carbon capture process, ORC operating conditions and mixture working fluid composition simultaneously. It is easy to add constraints for practical considerations, such as evaporation pressure limits. The results show that 4-stage compression performs best. The energy consumption can be reduced by 7.9% and one stage compression can be eliminated compared with the original design that does not include an ORC for the pre-compression of flue gas. Interestingly, a pure working fluid outperforms mixture working fluids for this 4-stage compression configuration. In other words, mixture working fluids do not always outperform pure working fluids. The results also suggest that a transcritical ORC may perform better due to a better thermal match, but heat exchanger design and system control are still challenging for transcritical ORCs. In future work, thorough investigation and comparison of transcritical and subcritical ORCs with mixture working fluids should be performed. In addition, this study does not consider uncertainty, which should be investigated in future work.

Acknowledgements

This publication has been funded by HighEFF—Centre for an Energy Efficient and Competitive Industry for the Future. The authors gratefully acknowledge the financial support from the Research Council of Norway and user partners of HighEFF, an 8-year Research Centre under the FME-scheme (Centre for Environment-friendly Energy Research, 257632/E20).

Appendix

General form of CEOS is as follows.

$$Z^3-(1+B-uB)Z^2+(A+wB^2-uB-uB^2)Z-AB-wB^2-wB^3=0$$

For the Peng-Robinson equation of state, $u=2, w=-1$.

where

$$Z=\frac{PV}{RT}$$

$$A=\frac{a^m P}{R^2T^2}$$

$$B=\frac{b^m P}{RT}$$

$$a^m=\sum_{i\in C}\sum_{j\in C}x_i x_j\sqrt{a_i a_j}\left(1-k_{ij}\right)$$

where k_{ij} is the binary interaction parameter.

$$b^m=\sum_{i\in C}x_i b_i$$

$$b_i=\frac{0.07780RT_{i,c}^2}{P_{i,c}}$$

$$a_i=\frac{\Omega_a R^2T_{i,c}^2}{P_{i,c}}\left[1+f^w(1-\sqrt{T/T_{i,c}})\right]^2$$

where $T_{i,c}$ and $P_{i,c}$ are the critical temperature and pressure of component i respectively.

$\Omega_a = 0.45724$ for Peng-Robinson equation of state.

$$f^w = 0.37464 + 1.54226\omega_i - 0.26992\omega_i^2$$

where ω_i is the acentric factor of component i.

Then the enthalpy and entropy can be calculated using departure functions.

$$h_s - h_s^0 = (a_s^m - T_s \frac{\partial a_s^m}{\partial T_s}) \frac{1}{b_s^m \sqrt{u^2 - 4\omega}} \ln\left[\frac{2Z_s + B_s(u - \sqrt{u^2 - 4\omega})}{2Z_s + B_s(u + \sqrt{u^2 - 4\omega})}\right] + RT_s(Z_s - 1)$$

$$S_s - S_s^0 = R\ln(\frac{Z_s + B_s}{Z_s}) + R\ln(\frac{Z_s P^0}{P_s}) - \frac{\partial a_s^m}{\partial T_s} \frac{1}{b_s^m \sqrt{u^2 - 4\omega}} \ln\left[\frac{2Z_s + B_s(u - \sqrt{u^2 - 4\omega})}{2Z_s + B_s(u + \sqrt{u^2 - 4\omega})}\right]$$

$$\frac{\partial a_s^m}{\partial T_s} = -\frac{R}{2}\sqrt{\frac{\Omega_a}{T_s}} \sum_{i \in C}\sum_{j \in C} x_i x_j (1 - k_{i,j}) \left[f_{\omega,j}\sqrt{\frac{a_i T_{j,c}}{P_{j,c}}} + f_{\omega,i}\sqrt{\frac{a_j T_{i,c}}{P_{i,c}}} \right]$$

$$h_s^0 = \sum_{i \in C} x_i \left[\frac{C_c^V}{5}(T^5 - T_0^5) + \frac{C_c^{IV}}{4}(T^4 - T_0^4) + \ldots + C_c^I (T - T_0) \right]$$

$$S_s^0 = \sum_{i \in C} x_i \left[\frac{C_c^V}{4}(T^4 - T_0^4) + \ldots + C_c^I \ln(\frac{T}{T_0}) \right]$$

where $C_c^V, C_c^{IV} \ldots C_c^I$ are specific constants related to the substance.

$$\ln(\phi_i) = \frac{b_i}{b_s^m}(Z - 1) - \ln(Z - B) + \frac{A}{B\sqrt{u^2 - 4\omega}}(\frac{b_i}{b_s^m} - \delta_i)\ln\left[\frac{2Z_s + B_s(u - \sqrt{u^2 - 4\omega})}{2Z_s + B_s(u + \sqrt{u^2 - 4\omega})}\right]$$

$$\frac{b_i}{b_s^m} = \frac{T_{i,c}/P_{i,c}}{\sum_{i \in C} x_i T_{i,c}/P_{i,c}}$$

$$\delta_i = \frac{2\sqrt{a_i}}{a_s^m} \sum_{j \in C} x_j \sqrt{a_j}(1 - k_{i,j})$$

Nomenclature

Symbols	
f	Molar flow rate
FCp	Heat capacity flowrate
H	Enthalpy
P	Pressure
$QSOA$	Heat load of hot streams above the pinch candidates
$QSIA$	Heat load of cold streams above the pinch candidates
S	Entropy
T	Temperature
Z	Compressibility factor
η	Efficiency
ΔT	Minimum heat transfer approach temperature
Superscripts	
L	Liquid phase
V	Vapor phase
p	Pinch candidate
Subscripts	
CU	Cold Utility
c	Component in the mixture
$comp$	Compressor
$mech$	Mechanical
HU	Hot Utility
i	State point in the ORC/ hot stream in the heat integration model
in	Inlet
is	Isentropic process
out	Outlet
$pump$	Pump
tur	Turbine
wf	Working fluid

shdw	Shadow stream
Acronyms	
ASU	Air Separation Unit
CPU	Compression and Purification Unit
CCS	Carbon Capture and Storage
CEOS	Cubic Equations of State
GAMS	General Algebraic Modeling System
GCC	Grand Composite Curve
IGCC	Integrated Gasification Combined Cycle
NGCC	Natural Gas Combined Cycle
LNG	Liquefied Natural Gas
ORC	Organic Rankine Cycle
Sets	
COMP	Compressors in the compression train
GSP	Gas state points
I	Hot streams
J	Cold streams
LSP	Liquid state points
PC	Pinch candidates
SP	State points

References

[1] C. Fu, T. Gundersen. Carbon Capture and Storage in the Power Industry: Challenges and Opportunities. Energy Procedia. 16, Part C (2012) 1806-12.
[2] M. Kanniche, R. Gros-Bonnivard, P. Jaud, J. Valle-Marcos, J.-M. Amann, C. Bouallou. Pre-combustion, post-combustion and oxy-combustion in thermal power plant for CO2 capture. Applied Thermal Engineering. 30 (2010) 53-62.
[3] C. Fu, T. Gundersen. Exergy Analysis and Heat Integration of a Coal-Based Oxy-combustion Power Plant. Energy & Fuels. 27 (2013) 7138-49.
[4] H. Yu, J. Eason, L.T. Biegler, X. Feng. Simultaneous heat integration and techno-economic optimization of Organic Rankine Cycle (ORC) for multiple waste heat stream recovery. Energy. 119 (2017) 322-33.

[5] J. Freeman, K. Hellgardt, C.N. Markides. An assessment of solar-powered organic Rankine cycle systems for combined heating and power in UK domestic applications. Applied Energy. 138 (2015) 605-20.
[6] Q. Liu, A. Shen, Y. Duan. Parametric optimization and performance analyses of geothermal organic Rankine cycles using R600a/R601a mixtures as working fluids. Applied Energy. 148 (2015) 410-20.
[7] Y. Jang, J. Lee. Optimizations of the organic Rankine cycle-based domestic CHP using biomass fuel. Energy Conversion and Management. 160 (2018) 31-47.
[8] H. Yu, X. Feng, Y. Wang, L.T. Biegler, J. Eason. A systematic method to customize an efficient organic Rankine cycle (ORC) to recover waste heat in refineries. Applied Energy. 179 (2016) 302-15.
[9] L.M. Romeo, Y. Lara, A. González. Reducing energy penalties in carbon capture with Organic Rankine Cycles. Applied Thermal Engineering. 31 (2011) 2928-35.
[10] P. Pei, K. Barse, A.J. Gil, J. Nasah. Waste heat recovery in CO2 compression. International Journal of Greenhouse Gas Control. 30 (2014) 86-96.
[11] G.G. Esquivel-Patiño, M. Serna-González, F. Nápoles-Rivera. Thermal integration of natural gas combined cycle power plants with CO2 capture systems and organic Rankine cycles. Energy Conversion and Management. 151 (2017) 334-42.
[12] M. Aneke, M. Wang. Potential for improving the energy efficiency of cryogenic air separation unit (ASU) using binary heat recovery cycles. Applied Thermal Engineering. 81 (2015) 223-31.
[13] U. Lee, C. Han. Simulation and optimization of multi-component organic Rankine cycle integrated with post-combustion capture process. Computers & Chemical Engineering. 83 (2015) 21-34.
[14] K. Kurtulus, A. Coskun, S. Ameen, C. Yilmaz, A. Bolatturk. Thermoeconomic analysis of a CO2 compression system using waste heat into the regenerative organic Rankine cycle. Energy Conversion and Management. 168 (2018) 588-98.
[15] H. Yu, X. Feng, Y. Wang. A new pinch based method for simultaneous selection of working fluid and operating conditions in an ORC (Organic Rankine Cycle) recovering waste heat. Energy. 90 (2015) 36-46.
[16] G. Angelino, P. Colonna di Paliano. Multicomponent working fluids for organic Rankine cycles (ORCs). Energy. 23 (1998) 449-63.
[17] J.L. Wang, L. Zhao, X.D. Wang. A comparative study of pure and zeotropic mixtures in low-temperature solar Rankine cycle. Applied Energy. 87 (2010) 3366-73.
[18] X.D. Wang, L. Zhao. Analysis of zeotropic mixtures used in low-temperature solar Rankine cycles for power generation. Solar Energy. 83 (2009) 605-13.
[19] F. Heberle, M. Preißinger, D. Brüggemann. Zeotropic mixtures as working fluids in Organic Rankine Cycles for low-enthalpy geothermal resources. Renewable Energy. 37 (2012) 364-70.
[20] M. Chys, M. van den Broek, B. Vanslambrouck, M. De Paepe. Potential of zeotropic mixtures as working fluids in organic Rankine cycles. Energy. 44 (2012) 623-32.
[21] Y. Zhou, F. Zhang, L. Yu. The discussion of composition shift in organic Rankine cycle using zeotropic mixtures. Energy Conversion and Management. 140 (2017) 324-33.
[22] H. Yu, T. Gundersen, X. Feng. Process integration of organic Rankine cycle (ORC) and heat pump for low temperature waste heat recovery. Energy. 160 (2018) 330-40.
[23] C. Fu, T. Gundersen. Using exergy analysis to reduce power consumption in air separation units for oxy-combustion processes. Energy. 44 (2012) 60-8.
[24] A.W. Dowling, C. Balwani, Q. Gao, L.T. Biegler. Optimization of sub-ambient separation systems with embedded cubic equation of state thermodynamic models and complementarity constraints. Computers & Chemical Engineering. 81 (2015) 323-43.
[25] B.A. McCarl, A. Meeraus, P. van der Eijk, M. Bussieck, S. Dirkse, P. Steacy, et al. McCarl GAMS user guide. Citeseer2014.
[26] A. Drud. GAMS/CONOPT. ARKI Consulting and Development, Bagsvaerd, Denmark. (1996).

[27] M.A. Duran, I.E. Grossmann. Simultaneous optimization and heat integration of chemical processes. AIChE Journal. 32 (1986) 123-38.
[28] A.W. Dowling, L.T. Biegler. A framework for efficient large scale equation-oriented flowsheet optimization. Computers & Chemical Engineering. 72 (2015) 3-20.
[29] R.S. Kamath, L.T. Biegler, I.E. Grossmann. An equation-oriented approach for handling thermodynamics based on cubic equation of state in process optimization. Computers & Chemical Engineering. 34 (2010) 2085-96.
[30] T. Gundersen. Numerical aspects of the implementation of cubic equations of state in flash calculation routines. Computers & Chemical Engineering. 6 (1982) 245-55.
[31] K. Satanphol, W. Pridasawas, B. Suphanit. A study on optimal composition of zeotropic working fluid in an Organic Rankine Cycle (ORC) for low grade heat recovery. Energy. 123 (2017) 326-39.
[32] H. Yu, X. Feng, Y. Wang. Working fluid selection for organic Rankine cycle (ORC) considering the characteristics of waste heat sources. Industrial & Engineering Chemistry Research. 55 (2016) 1309-21.
[33] H. Yu, J. Eason, L.T. Biegler, X. Feng. Process integration and superstructure optimization of Organic Rankine Cycles (ORCs) with heat exchanger network synthesis. Computers & Chemical Engineering. 107 (2017) 257-70.
[34] S. Balakrishna, L.T. Biegler. Targeting strategies for the synthesis and energy integration of nonisothermal reactor networks. Industrial & Engineering Chemistry Research. 31 (1992) 2152-64.
[35] R. Tian, Q. An, H. Zhai, L. Shi. Performance analyses of transcritical organic Rankine cycles with large variations of the thermophysical properties in the pseudocritical region. Applied Thermal Engineering. 101 (2016) 183-90.